RSC Advances

PAPER

View Article Online
View Journal | View Issue

Cite this: *RSC Adv.*, 2020, **10**, 23270

A porous nano-adsorbent with dual functional groups for selective binding proteins with a low detection limit

Xueyan Zou,[aef] Yu Zhang,[b] Jinqiu Yuan,[c] Zhibo Wang,[b] Rui Zeng,[c] Kun Li,[d] Yanbao Zhao*[aef] and Zhijun Zhang *[aef]

In this study, porous silica nanoparticles functionalized with a thiol group (SiO_2–SH NPs) were synthesized *via* a one-pot method. Subsequently, iminodiacetic acid was modified, and further adsorption of Ni^{2+} ions was conducted to obtain a SiO_2–S/NH–Ni nano-adsorbent. Then, transmission electron microscopy (TEM), scanning electron microscopy (SEM), Fourier transform infrared (FT-IR) spectroscopy, thermogravimetric analysis (TG) and X-ray diffraction (XRD) were employed to characterize its morphology and composition. The results indicate that the SiO_2–S/NH–Ni nano-adsorbent is porous, has an average diameter of 77.1 nm and has a small porous structure of about 3.7 nm in the silica skeleton. The Brunauer–Emmett–Teller (BET) surface area and total pore volume were 537.2 $m^2\ g^{-1}$ and 3.3 $cm^3\ g^{-1}$, respectively, indicating a large BET surface area. The results indicate that the as-prepared SiO_2–S/NH–Ni nano-adsorbent would be suitable to selectively and efficiently bind His-tagged proteins from an *E. coli* cell lysate. The SDS-PAGE results show that the as-prepared nano-adsorbent presents specifically to both His-tagged CPK4 and His-tagged TRX proteins, indicating the nano-adsorbent can be used to effectively separate His-tagged proteins and is universal to all His-tagged fusion proteins. We also found that the as-prepared nano-adsorbent exhibits a low detection limit (1.0×10^{-7} mol L^{-1}) and a strong regeneration ability based on four regeneration experiments that were particularly suited to the separation of His-tagged proteins.

Received 7th February 2020
Accepted 14th May 2020

DOI: 10.1039/d0ra01193b

rsc.li/rsc-advances

Introduction

Proteins play a variety of crucial roles in organisms, and the enrichment and purification of proteins, particularly low-abundance proteins, are currently hot topics.[1–6] Histidine is a semi essential amino acid for humans that constitutes the proteins of the body. It has a very wide range of applications, such as in food, medicine and other fields.[7–10] Furthermore, biotechnologies nowadays have enabled proteins to easily express with a tag, and numerous protein-purification methods are based on the specific interactions between immobilized ligands and affinity tags.[11–16] Among affinity tags, histidine tags are particularly popular as they can be readily incorporated into desired proteins by the expression of the target gene in micro-organism cells using commercial expression vectors.[17,18] Therefore, the easy separation and purification of His-tagged proteins are very important in biology and medicine.

Recently, metal-chelate affinity precipitation has been employed to separate His-tagged recombinant proteins based on the interactions between metal ions (Ni^{2+}, Cu^{2+}, Zn^{2+} and so on) and the histidine residues exposed on the surface of the proteins.[19–22] Although metal-chelate affinity precipitation is easily adaptable to any protein expression system, there are some limits to using this method, such as a requirement for pretreatment, solvent consumption, and protein solubility.[23–25]

With the development of nanotechnology, nanomaterials are used in many fields, such as protein purification, environmental treatment, targeted drugs and so on.[26–28] However, the major limitations of current nanomaterial systems are the detection limit and poor regeneration ability, which leads to low purification efficiency. In this study, porous silica with dual functional groups (–SH and $–NH_2$ groups) was employed as an adsorbent to separate His-tagged proteins. This material can provide a larger surface area, comparable to solid particles, and improve the separation capacity. The as-prepared nano-adsorbent can be used to directly separate His-tagged proteins from the *E. coli* lysate.

[a]*Engineering Research Center for Nanomaterials, Henan University, Kaifeng 475004, China. E-mail: zhangzj09@126.com; zhaoyb902@henu.edu.cn*
[b]*College of Chemistry and Chemical Engineering, Henan University, Kaifeng 475004, China*
[c]*Institute of Technology, Henan University Minsheng College, Kaifeng 459000, China*
[d]*State Key Laboratory of Crop Stress Adaptation and Improvement, Kaifeng 459000, China*
[e]*National & Local Joint Engineering Research Center for Applied Technology of Hybrid Nanomaterials, Kaifeng 459000, China*
[f]*Key Laboratory for Monitor and Remediation of Heavy Metal Polluted Soils of Henan Province, Jiyuan 459000, China*

Results and discussion

Fig. 1 shows the SEM (a) and TEM (b) images of the as-synthesized SiO_2–S/NH–Ni sample. It can be seen in Fig. 1a that the main products were spherical in shape and presented uniform spheres. Moreover, we could see that the as-prepared SiO_2–S/NH–Ni sample displayed a narrow size distribution and had an average diameter of 77.1 nm (Fig. 1c). Evidently, the surfaces of these nanospheres were rough, which may be due to the oriented growth and crystallinity.[27] As shown in Fig. 1b, the obtained SiO_2–S/NH–Ni sample displays a small porous structure, with about 3.7 nm, in the silica skeleton.

Fig. 2a shows the FT-IR absorption spectra of the as-prepared SiO_2–SH NPs (curve 1) and SiO_2–SH/NH_2 NPs (curve 2). In the FT-IR spectra, the peak at 3430 cm^{-1} is attributed to the –OH stretching vibration of porous silica spheres. The peaks at around 1105, 807 and 471 cm^{-1} were due to Si–O–Si stretching vibrations. The strong peaks at 2939 and 2836 cm^{-1} belong to the stretching vibrations of the $-CH_2-$ bonds in MPS, which indicates the presence of –SH in the SiO_2–SH NPs (Fig. 2a curve 1). It is clear that the curve of the SiO_2–SH/NH_2 NPs is very similar to that of the SiO_2–SH NPs, which indicates that the main component of SiO_2–SH/NH_2 NPs is SiO_2. The presence of the N–H bending vibration at around 695 cm^{-1} confirms the incorporation of the imino group of IDA.[29]

Fig. 2b shows the TG curve of the SiO_2–SH/NH_2 NPs. It can be seen that the sample displays successive weight loss from room temperature to 850 °C. The initial mass loss below 250 °C can be attributed to the desorption of adsorbed water from the surface of the sample powder, and the following mass loss was related to the further release of the inner adsorbed or crystal water (total mass loss 25%). The major mass loss (about 15.5%) took place in the range of 250–600 °C, which might be attributed to the thermal decomposition of the –SH and $-NH_2$ groups of the as-prepared SiO_2–SH/NH_2 NPs. This indicates that there are two groups (–SH and $-NH_2$) on the surface of the as-synthesized NPs. Fig. 2c shows the XRD pattern of the as-prepared SiO_2–SH/NH_2 NPs. The XRD pattern exhibits an obvious broad diffraction peak at around 23°, which was indexed to the scattering of amorphous SiO_2 (JCPDS 76-0933).[30]

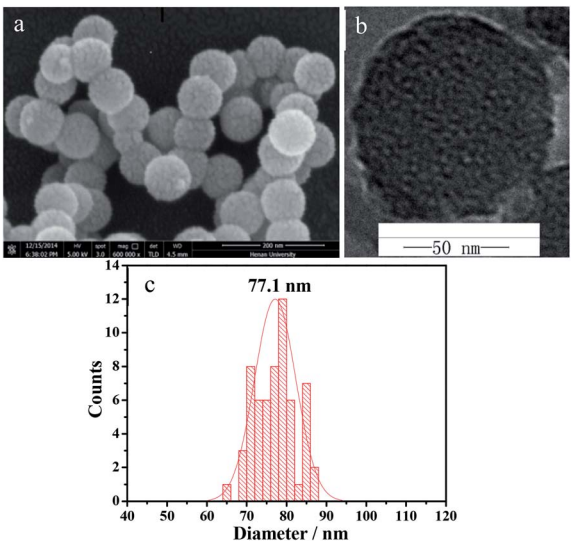

Fig. 1 SEM (a), TEM (b) images and distribution histogram (c) of the as-prepared SiO_2–S/NH–Ni NPs.

The surface and pore properties of the as-prepared SiO_2–SH/NH_2 NPs was examined *via* N_2 sorption, as shown in Fig. 3. It can be seen in Fig. 3a that the N_2 adsorption–desorption isotherms are characteristic of type IV curves with the H4 hysteresis loop in the relative-pressure range of 0.04–0.3, which indicates the presence of well-defined mesoporous structures with narrow slit-like pores.[31,32] It can be seen that the pore size distributions calculated using the BJH method were 3.3 and 3.7 nm (Fig. 3b). Moreover, the Brunauer–Emmett–Teller (BET) surface area and total pore volume were 537.2 $m^2\ g^{-1}$ and 3.3 $cm^3\ g^{-1}$, respectively, which represents a large BET surface area that is suitable for separating proteins.

Fig. 4 shows a scheme of the preparation of the SiO_2–S/NH–Ni nano-adsorbent and their separation of His-tagged proteins. It can be seen that there are three steps required to synthesize the SiO_2–S/NH–Ni nano-adsorbent. First, SiO_2–SH was prepared by the hydrolysis of TEOS and MPS *via* a one-pot method. Second, the IDA molecules were modified on the surfaces of the SiO_2–SH NPs. Third, the SiO_2–S/NH–Ni nano-adsorbent was obtained by chelating Ni^{2+}. Then, the nano-adsorbent can be used to separate His-tagged proteins from the *E. coli* lysate, and the obtained SiO_2–S/NH–Ni/His-tagged proteins can be eluted by imidazole. Subsequently, the His-tagged proteins can be obtained, and the remaining SiO_2–S/NH–Ni nano-adsorbent could be reused by regeneration with EDTA and $NiCl_2$ solutions. The results show that the as-prepared SiO_2–S/NH–Ni nano-adsorbent has a strong regeneration ability, particularly suited to the separation of the His-tagged fusion proteins.

To estimate the separation effect of the as-prepared samples, SDS-PAGE was employed as a general method for assessing the target proteins. Fig. 5 shows the SDS-PAGE analysis of His-tagged proteins that were purified by the SiO_2–S/NH–Ni nano-adsorbent. Lanes 1–4 contain the fractions washed off from the SiO_2–S/NH–Ni nano-adsorbent with different amounts of imidazole (lane 1, 0.5 mol L^{-1}; lane 2, 1 mol L^{-1}; lane 3, 2 mol L^{-1}; lane 4, 3 mol L^{-1}). Lane 5 contains the marker, and lane 6 contains the *E. coli* lysate. It was been found that the SiO_2–S/NH–Ni nano-adsorbent could efficiently enrich target proteins from cell lysate. By changing the concentration of imidazole (0.5–3 mol L^{-1}) and keeping the others unchanged, the quantity of disassociated proteins remained basically the same with increment in the concentration of imidazole (Fig. 5 lane 1–4), so 0.5 mol L^{-1} imidazole was used in subsequent experiments.

Keeping the imidazole concentration constant (0.5 mol L^{-1}), the effect of the concentration of the target proteins was investigated, as shown in Fig. 5. The concentrations in the lanes 7–10 are as follows: lane 7, 1.0×10^{-4} mol L^{-1}; lane 8, 1.0×10^{-5} mol L^{-1}; lane 9, 1.0×10^{-6} mol L^{-1}; lane 10, 1.0×10^{-7} mol L^{-1}; lane 11, 1.0×10^{-8} mol L^{-1}. When the concentrations of the TRX proteins were 1.0×10^{-4}, 1.0×10^{-5}, 1.0×10^{-6}, 1.0×10^{-7} and 1.0×10^{-8} mol L^{-1}, the target proteins

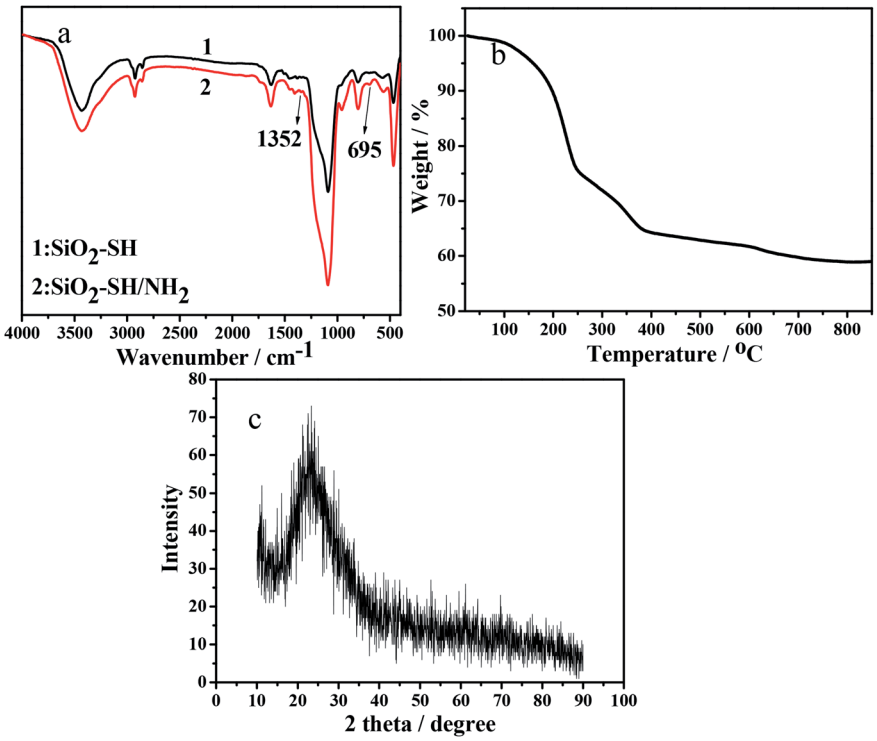

Fig. 2 FT-IR spectrum (a), TG curve (b) and XRD pattern (c) of the SiO_2–SH/NH_2 NPs.

could be detected effectively by the as-prepared SiO_2–S/NH–Ni nano-adsorbent, which shows that the samples can be used to detect target proteins with a detection limit lower than 1.0×10^{-7} mol L^{-1}.

In order to investigate the reusability properties of the as-prepared SiO_2–S/NH–Ni nano-adsorbent, we separated the target proteins four times. Fig. 6 shows the SDS-PAGE for the four recycling times using lane 1, Ni-NTA agarose; lane 2, marker; lane 3, His-tagged TRX *E. coli* lysate; lane 5, 1st; lane 6, 2nd; lane 7, 3rd; lane 8, 4th. The adsorbent could be repeatedly used in the experiment if it was treated with EDTA and $NiCl_2$ as needed. It can be seen that the specificity and affinity of the SiO_2–S/NH–Ni nano-adsorbent remained unaffected after four recycling times. The binding capacities of the target protein were 9.8, 9.8, 9.6 and 9.2 mmol g^{-1}.

In order to verify the universality of the SiO_2–S/NH–Ni nano-adsorbent, we used the adsorbent to separate His-tagged Ca^{2+}-dependent protein kinase 4 (His-tagged CPK4) proteins from the *E. coli* lysate, as shown in Fig. 6. The lanes are as follow: lane 3, His-tagged TRX *E. coli* lysate; lane 4, His-tagged CPK4 *E. coli* lysate; lane 9, His-tagged TRX separated by the SiO_2–S/NH–Ni nano-adsorbent; lane 10, His-tagged CPK4 separated by the SiO_2–S/NH–Ni nano-adsorbent. It is clear that the His-tagged CPK4 proteins could be separated specifically from the *E. coli* lysate, and there was no nonspecific binding. These results indicate that the as-prepared SiO_2–S/NH–Ni nano-adsorbent could be used effectively in His-tagged protein affinity separation or purification, and it is universally applicable to all His-tagged fusion proteins. These results are due to the Ni of the as-prepared SiO_2–S/NH–Ni nano-adsorbent being specific to

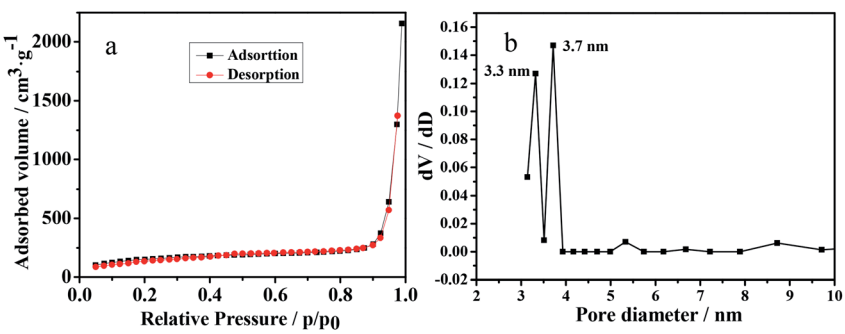

Fig. 3 N_2 adsorption–desorption isotherm (a) and the pore size distribution (b) of the SiO_2–S/NH–Ni NPs.

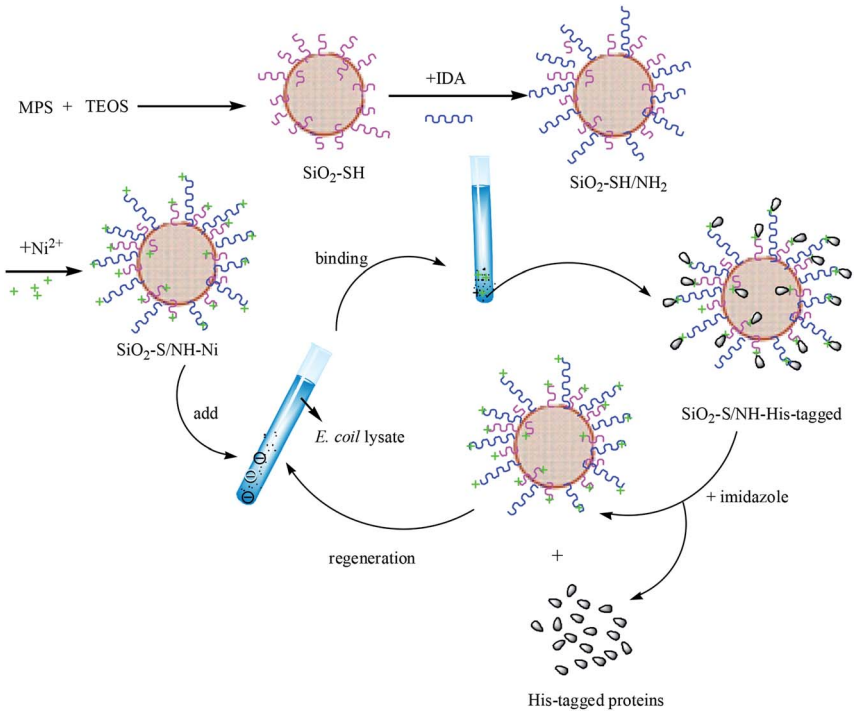

Fig. 4 Scheme for the preparation of the SiO_2–S/NH–Ni samples and their separation of His-tagged proteins.

histidine and the specific binding being independent of the type of fusion proteins.

Experimental

Materials

Ni-NTA agarose was purchased from QIAGEN. Phosphate buffer saline solutions (abridged as PBS; concentration 0.1 mol L^{-1}, pH = 8.0; concentration 0.01 mol L^{-1}, pH = 7.4) were purchased from Sigma-Aldrich, America. 3-Glycidyloxy-propyltrimethoxysilane (GPTMS) and iminodiacetic acid (IDA) were purchased from Aladdin. Tetraethyl orthosilicate (TEOS) was from Tianjin Fuchen Chemicals. 3-Mercaptopropyltrimethoxysilane (MPS) was supplied from Alfa-Aesar. Hexadecyl-trimethylammonium bromide (CTAB) was from Sinopharm Chemicals. Triethanolamine (TEA), ethylene diamine tetraacetic acid (denoted as EDTA), absolute alcohol and aqueous ammonia (28 wt%) were purchased from Tianjin Kermel Chemicals.

Synthesis of the SiO_2–S/NH–Ni nano-adsorbent

In a typical synthesis, 93.75 μmol of CTAB was added into 19 mL of an ethanol solution (v(CH_3CH_2OH)/v(H_2O) = 6 : 1) and stirred for a few minutes. Then, 1.1 mL of TEA was also added into

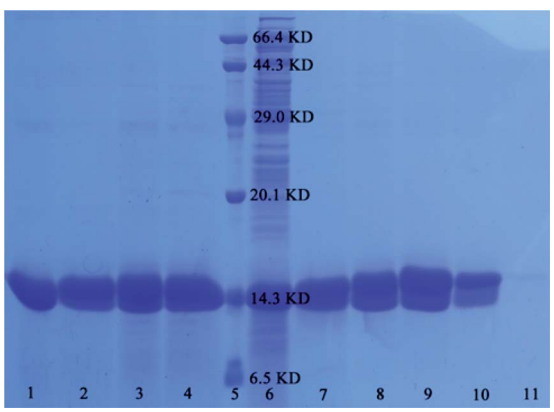

Fig. 5 SDS-PAGE analysis of His-tagged proteins separated by the SiO_2–S/NH–Ni nano-adsorbent.

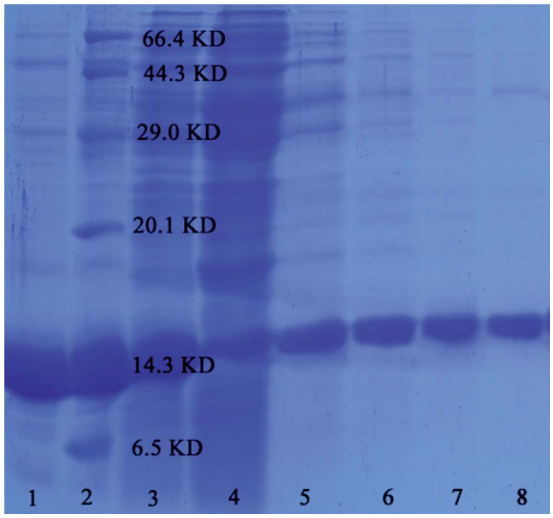

Fig. 6 SDS-PAGE analysis of His-tagged proteins separated by the as-prepared SiO_2–S/NH–Ni nano-adsorbent.

the above solution. Subsequently, 1.54 mL of the mixed solution of TEOS and MPS (v/v = 10 : 1) was dropped slowly into the above solution at 60 °C (28 μL s^{-1}) and reacted for 3 h. Then, the precipitate was treated with an ethanol–HCl solution for 12 h to remove the CTAB template and was then washed with deionized water three times and dried for 48 h at 60 °C to obtain SiO_2–SH NPs.

Then, 20 mL of an IDA solution (0.085 g mL^{-1}, pH = 11) was added into a flask, and the solution was kept at 0 °C in an ice-bath. Then, 2 mL of GPTMS was added under stirring conditions, and the mixture was reacted at 65 °C for 12 h. Subsequently, 0.2 g of SiO_2–SH NPs was dispersed in 6 mL of the GPTMS-IDA solution (pH = 2), and the suspension was sustained at 90 °C for 3 h. Finally, the suspension was centrifuged, washed and dried to get SiO_2–SH/NH_2 NPs. For chelating the Ni^{2+} ions, 5 mg of SiO_2–SH/NH_2 NPs was dispersed in 50 mL of a 0.2 mol L^{-1} $NiCl_2$ solution and reacted at 25 °C for 24 h. Then, the SiO_2–S/NH–Ni nano-adsorbent was washed by deionized water for several times and stored at 4 °C.

Affinity separation of His-tagged proteins

After being washed with a 0.02 mol L^{-1} Tris–HCl binding buffer three times, the SiO_2–S/NH–Ni nano-adsorbent was dispersed directly into 1 mL of *E. coli* lysate and shaken for 2 h at a rotation speed of 70 rpm at 4 °C. Then, the SiO_2–S/NH–Ni nano-adsorbent with the captured His-tagged proteins was washed with Tris–HCl buffer three times to remove any residual uncaptured proteins. Finally, the SiO_2–S/NH–Ni nano-adsorbent with the captured His-tagged proteins was eluted with 0.3 mL of 0.05 mol L^{-1} imidazole solution. The SiO_2–S/NH–Ni nano-adsorbent can be recovered and reused by washing sequentially with 0.1 mol L^{-1} EDTA and 0.2 mol L^{-1} $NiCl_2$ solutions.

Characterization

Transmission electron microscopy (TEM, JEM-2010), scanning electron microscopy (SEM, JSM 5600LV), Fourier transform infrared spectroscopy (FT-IR, AVATAR360) and thermogravimetric analysis (TG, EXSTAR 6000) were employed to detect the morphology and composition of the as-prepared nanomaterials. The surface area was measured *via* the Brunauer–Emmett–Teller method (BET, QUADRASORB). The separated His-tagged proteins were detected with sodium dodecylsulfate polyacrylamide gel electrophoresis (SDS-PAGE, Power PAC 300). The concentration of the target proteins was analyzed at 280 nm on a UV-Vis spectrophotometer (UV-Vis, nanodrop 2000c).

Conclusions

In this study, thiol-functionalized porous silica nanoparticles were synthesized *via* a one-pot method. Then, the SiO_2–SH NPs were further modified by iminodiacetic acid and chelating Ni^{2+} ions to get the porous affinity absorbent, which could then be applied to separate His-tagged proteins. The results showed that the as-prepared absorbent had good specificity and regeneration ability for use with His-tagged fusion proteins. Moreover, the SiO_2–SH NP absorbent had high sensitivity to His-tagged proteins, and the detection limit for the target proteins was lower than 1.0×10^{-7} mol L^{-1}.

Conflicts of interest

There are no conflicts to declare.

Acknowledgements

The authors acknowledge the financial support provided by the National Natural Science Foundation of China (grant no. 21571051), the Science and Technology Department of Henan Province (in the name of "Major Science and Technology Project", grant no. 181100310600), Henan University (in the name of "Interdisciplinary Research for First-Class Discipline Construction Project", grant no. 2019YLXKJC04), Henan University Minsheng College (in the name of "Innovative Experimental and Practical Projects for College Students", grant no. MSCXSY2019007 and MSCXSY2019016).

Notes and references

1 W. Li, F. A. Zhao, W. P. Fang, D. Y. Xie and J. N. Hou, *Front. Plant Sci.*, 2015, **6**, 732–745.
2 L. Q. Chai, J. H. Meng, J. Gao, Y. H. Xu and X. W. Wang, *Fish Shellfish Immunol.*, 2018, **80**, 155–164.
3 J. F. Hua, S. Zhang, J. J. Cui, D. J. Wang and C. Y. Wang, *J. Insect Physiol.*, 2013, **59**, 690–696.
4 M. Y. Chen, K. Li, H. P. Li, C. P. Song and Y. C. Miao, *Sci. Rep.*, 2017, **7**, 44743–44757.
5 S. S. Liang, L. Xiao, P. H. Huang, Z. Y. Cheng, F. L. Chen, Y. C. Miao, Y. F. Fu and Q. S. Chen, *Plant Cell Rep.*, 2019, **38**, 1263–1271.
6 L. Li, M. J. Hou, L. Cao, Y. Xia and Z. G. Shen, *Environ. Exp. Bot.*, 2018, **155**, 313–320.
7 B. K. Oh, S. Park, J. E. Millstone, S. W. Lee, K. B. Lee and C. A. Mirkin, *J. Am. Chem. Soc.*, 2006, **128**, 11825.
8 J. H. Lee, Y. M. Huh, Y. W. Jun, J. W. Seo, J. T. Jang, H. T. Song, S. Kim, E. J. Cho, H. G. Yoon, J. S. Suh and J. Cheon, *Nat. Med.*, 2007, **13**, 95–99.
9 D. Driss, F. Bhiri, R. Ghorbel and S. E. Chaabouni, *Protein Expression Purif.*, 2012, **83**, 8–14.
10 M. Mielecki, J. Wojtasikb, M. Zborowskab, K. Kurzatkowska, K. Grzelak, W. Dehaen, J. Radecki and H. Radecka, *Electrochim. Acta*, 2013, **96**, 147–154.
11 K. J. Lei, Y. Lin, J. Ren, L. Bai and Y. C. Miao, *Plant Cell Physiol.*, 2016, **57**, 192–203.
12 M. Perrier, M. Gary-Bobo, L. Lartigue, D. Brevet, A. Alain Morère, M. Garcia, P. Maillard, L. Raehm, Y. Guari, J. Larionova, J. O. Durand, O. Mongin and M. J. Blanchard-Desce, *J. Nanopart. Res.*, 2013, **15**, 1602–1618.
13 P. C. Wang, Y. Y. Du, Y. J. Hou, Y. Zhao and C. C. P. Hsu, *Proc. Natl. Acad. Sci. U. S. A.*, 2015, **112**, 613–618.
14 D. R. Bae, S. J. Lee, S. W. Han, J. M. Lim, D. M. Kang and J. H. Jung, *Chem. Mater.*, 2008, **20**, 3809–3813.

15 X. Zhao, J. Wang, J. Yuan, X. L. Wang and Q. P. Zhao, *New Phytol.*, 2015, **207**, 211–224.
16 N. Li, X. Sun and M. Q. J. Wang, *J. Appl. Entomol.*, 2017, **141**, 751–757.
17 Y. B. Yin, G. M. Wei, X. Y. Zou and Y. B. Zhao, *Sens. Actuators, B*, 2015, **209**, 5108–5511.
18 X. Y. Zou, K. Li, Y. B. Yin, Y. B. Zhao, Y. Zhang, B. J. Li, S. S. Yao and C. P. Song, *Mater. Sci. Eng., C*, 2014, **34**, 468–473.
19 F. Xu, J. H. Geiger, G. L. Baker and M. L. Bruening, *Langmuir*, 2011, **27**, 3106–3112.
20 X. Y. Zou, K. Li, Y. B. Yin, Y. B. Zhao, Y. Zhang, B. J. Li, S. S. Yao and C. P. Song, *Mater. Sci. Eng., C*, 2014, **34**, 468–473.
21 W. J. Fang, X. L. Chen and N. F. Zheng, *J. Mater. Chem.*, 2010, **20**, 8624–8630.
22 W. B. Yap, B. T. Tey, N. B. M. Alitheen and W. S. Tan, *J. Chromatogr. A*, 2010, **1217**, 3473–3480.
23 C. J. Xu, K. M. Xu, H. W. Gu, X. F. Zhong, Z. H. Guo, R. K. Zheng, X. X. Zhang and B. Xu, *J. Am. Chem. Soc.*, 2004, **126**, 3392–3393.
24 K. S. Lee and I. S. Lee, *Chem. Commun.*, 2008, **14**, 709–711.
25 B. Mizrahi, S. Irusta, M. Mckenna, C. Stefanescu, L. Yedidsion, M. Myint, R. Langer and D. S. Kohane, *Adv. Mater.*, 2011, **23**, H258–H262.
26 Y. Y. Wang, Y. D. Liu, W. H. Zhan, K. X. Zheng, J. N. Wang, C. S. Zhang and R. H. Chen, *Sci. Total. Environ.*, 2020, **729**, 139060.
27 X. Y. Zou, K. Li, Y. B. Zhao, Y. Zhang, B. J. Li and C. P. Song, *J. Mater. Chem. B*, 2013, **1**, 5108–5113.
28 Y. Y. Wang, Y. D. Liu, W. H. Zhan, K. X. Zheng, M. M. Lian, C. S. Zhang, X. L. Ruan and T. Li, *Ecotoxicol. Environ. Saf.*, 2020, **197**, 110600.
29 M. F. Jeng, A. P. Campbell, T. Begley, A. Holmgren, D. A. Case, P. E. Wright and H. J Dyson, *Structure*, 1994, **2**, 853–868.
30 H. Zhu, B. Lee, S. Dai and S. H. Overbury, *Langmuir*, 2003, **19**, 3974–3980.
31 S. S. Wu, X. Huang and X. Z. Du, *J. Mater. Chem. B*, 2015, **3**, 1426–1432.
32 S. Q. Liu, M. Y. Wei, J. C. Rao, H. X. Wang and H. Zhao, *Mater. Lett.*, 2011, **65**, 2083–2085.